

First-principles design for strain-tunable exciton dynamics in 2D materials

Amir Kleiner¹ and Sivan Refaely-Abramson¹

¹*Department of Molecular Chemistry and Materials Science,
Weizmann Institute of Science, Rehovot 7610001, Israel*

(Dated: July 15, 2025)

Abstract

Controlling exciton motion in two-dimensional semiconductors is key to unlocking new optoelectronic and straintronic functionalities. Monolayer transition metal dichalcogenides (TMDs), with their tightly bound excitons, offer an ideal platform for such control due to their strong sensitivity to local strain. Here we present an ab initio framework for modeling exciton dynamics in inhomogeneously strained WS_2 , combining excitonic band structures derived from first principles with a semiclassical transport model operating in both real and momentum space. By analyzing idealized strain patterns, we reveal how excitons undergo drift, diffusion, and confinement without invoking empirical parameters. Our results uncover regimes of super-ballistic propagation and negative effective diffusion, governed entirely by the strain landscape. This work provides microscopic insight into strain-tunable exciton behavior and establishes design principles for engineering exciton flow in two-dimensional materials.

The electronic band structure of quantum particles in periodic solids is defined by their energy dispersion with crystal momentum, $E(\mathbf{k})$. Transition metal dichalcogenides (TMDs) are a class of wide band-gap semiconductors whose optoelectronic properties are strongly layer-dependent. While bulk TMDs exhibit an indirect gap, monolayer (ML) forms possess a direct band gap, with both the conduction and valence band extrema shifting between the two limits [1, 2]. Monolayer TMDs have emerged as a versatile platform for engineering quantum phenomena, owing to their structural tunability via chalcogen vacancies [3–5], heterostructure design [6–8], and control over twist angles and moiré superlattices [9–11].

Among the most powerful and versatile strategies for tuning the properties of TMD monolayers is the application of in-plane strain, which provides a continuous and controllable means of modulating both electronic and excitonic behavior. Monolayer TMDs can sustain strains exceeding $\sim 11\%$ without mechanical failure or phase transitions [12, 13], and their band structures exhibit pronounced sensitivity to such deformations. Applied strain shifts both the positions and curvatures of band extrema [12–14], with effects that vary across the Brillouin zone and enable smooth transitions between direct and indirect band gaps [14, 15]. The excitonic band structure is similarly strain-sensitive, showing tunable dispersion and energy shifts under deformation [16]. While this general strain response is consistent across all semiconducting TMD monolayers [17, 18] and many multilayer systems [19, 20], the precise strain dependence and the critical strain for gap transitions vary with composition

and thickness [21–23].

Spatially varying strain in monolayer TMDs—i.e., inhomogeneous or non-uniform strain profiles—can actively drive exciton dynamics in the material [12, 24–27], enabling exciton trapping and guiding via strain-engineered potentials [20, 28–30]. These strain-induced effects manifest as exciton drift driven by energy gradients [12, 25], as well as strain-induced diffusion [24]. Exciton transport in such systems has typically been modeled using phenomenological drift-diffusion equations, where position- and time-dependent mobility and diffusion coefficients are fitted to experimental or empirical trends [24, 31]. Drift is commonly attributed to the strain-induced spatial variation of exciton energies—driving excitons toward regions of lower energy (higher strain) [12, 24]. Diffusion behavior, in contrast, has drawn considerable attention due to reports of anomalous [32–34] and even “negative” diffusion regimes [35]. Yet most theoretical treatments rely on simplified models that either neglect the composite quasiparticle nature of excitons [23, 36, 37], or use first principles results only to parametrize otherwise phenomenological transport models [32, 38, 39]. In particular, excitonic dispersion is often approximated using strain-independent effective masses, and energies are typically evaluated only at high-symmetry k-points [32, 34]. While such approaches can capture complex many-body processes—such as intervalley scattering [36, 37] or trion formation [31, 40]—they often neglect the full momentum-space structure of the exciton under strain, limiting their ability to reveal the microscopic mechanisms driving exciton transport in strained 2D materials.

In this work, we develop a first-principles-based semiclassical framework to model exciton dynamics in inhomogeneously strained monolayer transition metal dichalcogenides (TMDs), treating exciton propagation on a real- and momentum-space potential energy surface derived entirely from *ab initio* calculations. By simulating exciton motion under idealized strain landscapes, we isolate the impact of band curvature and energy gradients on drift, confinement, and diffusion, revealing how strain governs distinct transport regimes. Our approach, applicable to quasiparticles in systems of arbitrary dimensionality where the band structure evolves continuously with strain, establishes a general foundation for *ab initio*-guided design of strain-controlled excitonic and quantum transport in next-generation materials and devices.

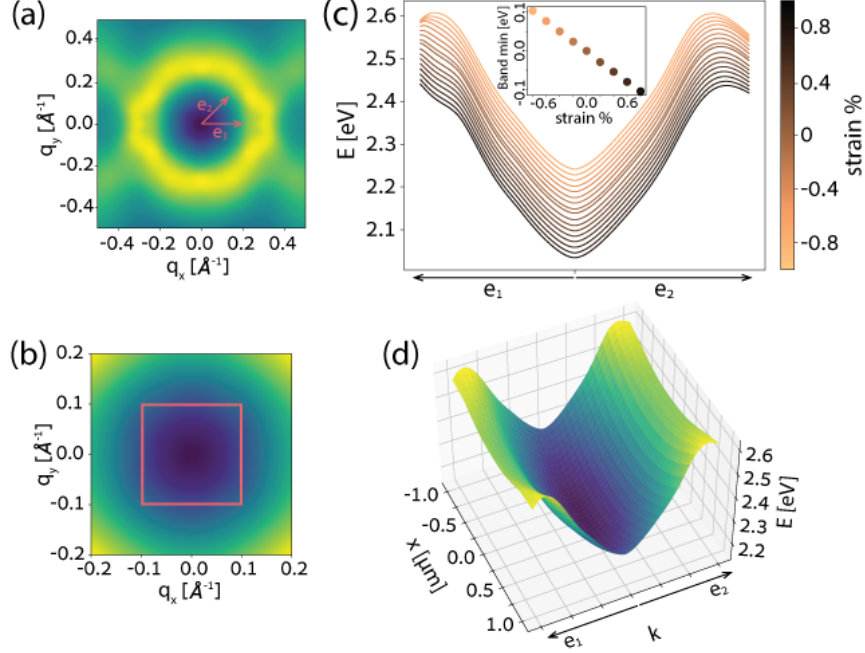


FIG. 1. (a) First bright excitonic band centered around the Γ center-of-mass momentum with paths utilized for line-plot marked as e_1 and e_2 . (b) Close-up of the parabolic region of the band, with the region utilized for the dynamics simulations marked by a red square. (c) First bright excitonic band along the e_1 and e_2 directions, plotted for various strains. (inset) position of the band minimum for various strains. The exciton band minimum exhibits an inverse proportionality for the range of strains utilized in this study. (d) Illustration of a 2D slice of the full potential, with a concave parabolic strain profile along one direction in position space, and a path along e_1 and e_2 in momentum space, representing the (1,1) and (1,-1) directions in crystal axes.

STRAINED AND POSITION-DEPENDENT BAND STRUCTURES

The atomic arrangement in TMD monolayers follows a hexagonal symmetry, which is inherited by both the electronic and excitonic band structures. The excitonic bands of TMDs also have a hexagonal symmetry, as is shown in Figure 1 (a). Near the Γ -point (zero center-of-mass momentum), the first bright exciton band exhibits a parabolic dispersion [41], as is shown in figure 1 (b). Applying strain to the monolayer modulates both the curvature of the exciton dispersion and the absolute energy of the band minimum. The strains computed in this study, in the range of -0.8% to $+0.8\%$ applied to the whole unit cell, have a negligible effect on the effective masses close to Γ , though the effect gets more

pronounced further away from Γ . At this range of strains, the shift in the energy of the band edge is linear with strain, and has a magnitude of 129.6 meV%. These trends are showcased in Figure 1 (c).

When an inhomogeneous strain profile is applied to a large layer, the shape of each unit cell is altered. However, provided that the strain gradient is small compared to the unit cell size, then locally the changes are negligible, and a local band structure approximation remains valid. This assumption enables the construction of a position-dependent band structure by interpolating the strained band structures across a continuous strain field. For a 2D layer, this results in a 4D potential $E(\vec{r}, \vec{q})$ that explicitly depends on both the two position-space coordinates \vec{r} and the two crystal momentum-space coordinates \vec{q} . Figure 1 (d) shows a 2D slice through one such 4D potential surface, combining a 1D concave parabolic strain profile along position space with a momentum-space cut through the Brillouin zone. The resulting energy landscape reflects the anisotropic and nonlinear coupling between strain and exciton dynamics. Further details of the interpolation procedure are provided in the SI. This interpolated potential forms the basis of the exciton dynamics model introduced in the next section, allowing us to evaluate how strain-induced band structure variations translate into spatial exciton behavior.

Experimentally, strain profiles can be induced in materials by various methods - e.g. by applying direct forces through an AFM cantilever [12, 31, 42] or multi-point bending apparatus [43], pressurizing an airtight cavity with a monolayer TMD as a membrane [44], patterning and imprinting [38, 45], wrinkling [42, 46] or electrostatic forces [39]. Each method results in drastically different strain profiles. Here we restrict our study to simple polynomial strain profiles, aiming to elucidate the physical principles behind the strain-induced dynamics.

DYNAMICS MODEL

We model the dynamics of a macroscopic exciton distribution $n(\vec{r}, \vec{q})$, initialized by an optical excitation characterized by a spread in momentum around the center-of-mass $\vec{q} = 0$, consistent with the light cone of the excitation source. The evolution of this distribution on the position- and momentum-dependent potential energy surface is governed by the following

general equation of motion (EOM):

$$\begin{aligned} \frac{\partial n_X(\vec{r}, \vec{q}, t)}{\partial t} = & \\ & \nabla_{\vec{q}} n_X(\vec{r}, \vec{q}, t) \cdot \nabla_{\vec{r}} E(\vec{r}, \vec{q}) \\ & - \nabla_{\vec{r}} n_X(\vec{r}, \vec{q}, t) \cdot \nabla_{\vec{q}} E(\vec{r}, \vec{q}) \\ & + K_{ext}[n(\vec{r}, \vec{q}), \vec{r}, \vec{q}, t]. \end{aligned} \quad (1)$$

The last term, K_{ext} incorporates all external interactions such as exciton-phonon and exciton-exciton scattering, interband crossings, and spontaneous radiative decay. We neglect these effects and focus on the ballistic regime, where dynamics are governed solely by the ab initio strain-induced excitonic potential surface. Further details on the development of the EOM are provided in the SI. Equation 1 constitutes a semiclassical approximation to the exciton dynamics, appropriate for modeling the evolution of macroscopic exciton ensembles, as often probed in experimental studies and envisioned in excitonic device applications. The approach is not suitable for describing single-exciton dynamics or coherent wavepacket evolution, where quantum effects such as interference and entanglement are essential.

The position and momentum-dependent potential does not, in general, correspond to a conservative force. The variation of the strain with position introduces effective forces that redistribute the exciton ensemble in both position and momentum space. This not only drives drift in position space but also evolves the momentum distribution, enabling us to track how exciton dynamics emerge from strain-induced band structure modulations. Our framework thus offers a clean probe of strain-induced band structure dynamics, without the need to include scattering with phonons, excitons, or other particles in the system. The total energy of the distribution, however, is conserved under the ballistic limit of the EOM. This results in a confinement of the momentum-space distribution for small strain values such as those studied in this work. The introduction of larger strains, in which the band minimum of one strain is higher in energy than the maximum between valleys in another strain, coupled with an appropriate potential and appropriate initiation of the distributions, should result in a phonon-independent mechanism for valley dynamics.

The potential energy surface was evaluated on a square real-space grid spanning $2\mu\text{m} \times 2\mu\text{m}$ with 20nm resolution, and a momentum-space grid from -0.1 \AA^{-1} to 0.1 \AA^{-1} with $2 \times 10^{-3} \text{ \AA}^{-1}$ resolution. Strain profiles were chosen to span the computed range of uniform strain values ($\pm 0.8\%$) without extrapolation.

The profiles studied have the general shape

$$s(x, y) = a_0 + a_1x + a_2x^2 + a_3x^3 + b_1y + b_2y^2 + b_3y^3 \quad (2)$$

where we can define separately *linear*, parabolic *concave*, parabolic *convex*, or *cubic* profile for each position coordinate. An initial exciton distribution was then initialized in various positions on the surfaces, with varying widths in the range of 30 – 50 nm, which corresponds to a photon beam of width 100 – 170 nm, which is about 2 times smaller than the diffraction limit for a laser in resonance with the unstrained A exciton. In momentum space the distribution was initialized around 0-momentum, with width varying in the range of 3×10^{-2} to 2.5×10^{-3} , which correspond to a distribution between an order of magnitude and a factor of 2 larger than the cone of light for a laser in resonance with the unstrained A exciton. Both widths have been chosen due to numerical stability considerations. While the simulations are not meant to quantitatively replicate experimental conditions, they provide valuable qualitative insight into the ballistic transport regimes relevant for strain-engineered exciton dynamics.

The time evolution of the distribution is evaluated using a 4th-order Runge-Kutta method, with 5th-order error estimations (RK45), while the static right-hand side of the equation is computed explicitly after each time step. We run the simulation for a total of ~ 1.5 ps. The temporal resolution is automatically determined by the RK45 solver, with a typical step of 1-10 fs.

RESULTS

We generated 11 distinct inhomogeneous strain profiles by activating individual polynomial components in each spatial dimension of Eq. 2. For each profile, we initialized 18 exciton distributions with varying spatial positions and momentum-space widths, allowing systematic exploration of how both strain geometry and initial conditions shape exciton dynamics.

Figure 2 illustrates representative cases of exciton propagation under combined strain profiles: convex or concave variation in the X-direction, coupled with linearly increasing or decreasing strain in the Y-direction. The evolution of the exciton distribution in both position and momentum space is shown as 50% height contours at multiple time steps, with

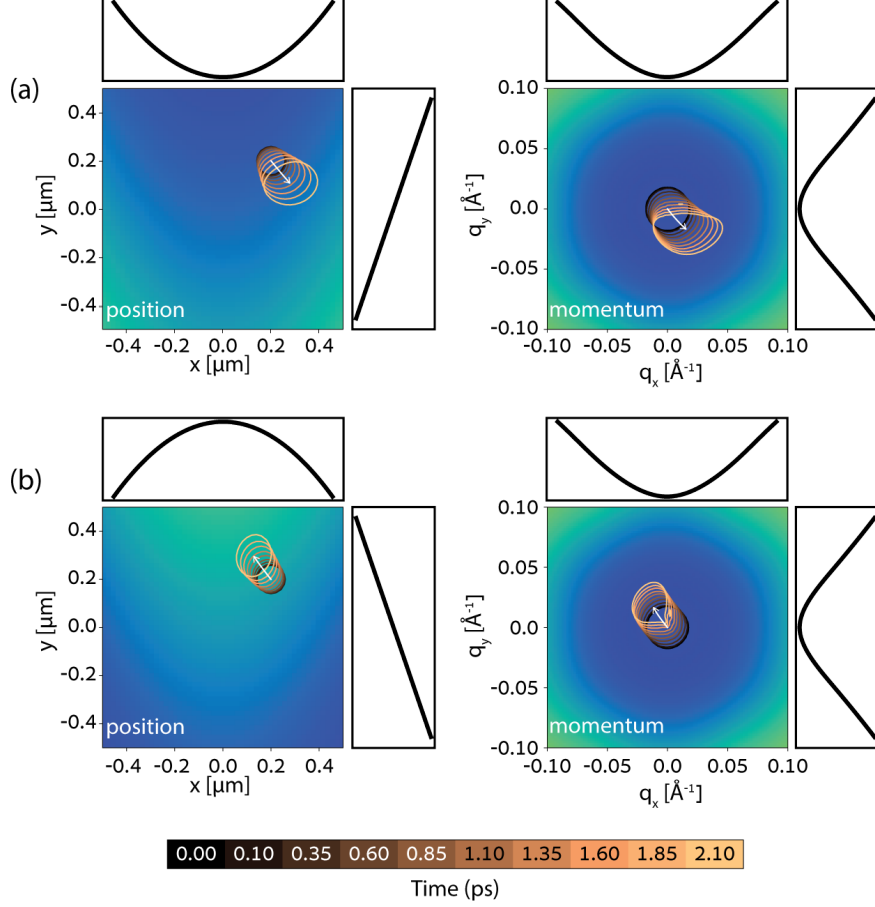


FIG. 2. Time evolution of the exciton distributions, expressed as the contour at 50% height for multiple time-steps and the propagation of the COM as a white arrow in position space (left) and momentum space (right) for (a) a parabolic convex in X and linear ascending in Y and (b) a parabolic concave in X and linear descending in Y strain profiles. Position-space backgrounds illustrate the appropriate strain profile. Low strain values are in blue, and high values are in green. As a guide to the eye, the projections along the axes are illustrated along the appropriate axes. Momentum-space backgrounds illustrate the average excitonic band. Low energy values are in blue, and high values are in green. As a guide to the eye, the projections along the axes are illustrated along the appropriate axes.

white arrows tracking the distributions' center-of-mass (COM) trajectory. The position-space background schematically illustrates the strain profile present in the system, while the momentum-space background schematically illustrates the average excitonic band in the system. In both cases, low-strain/energy values are represented in blue, and high-strain/energy values are represented in green. More detailed snapshots of the dynamics are

presented in the SI.

The coupling between real- and momentum-space components in the strain-induced potential results in complex propagation behavior, including significant distortion of the distribution in both domains. The COM of the distribution is used to track and analyze the drift elements of the dynamics. Consistent with experimental observations [24, 29], the exciton distributions exhibit directional drift toward regions of higher strain. The total drift depends largely on the type of strain profile and initial conditions. The maximal drift distance observed throughout the simulation is $0.18\mu\text{m}$, which results in a maximal average drift velocity of $1.20 \times 10^2 \mu\text{m}/\text{ns}$. The resulting drift velocity of approximately $120\mu\text{m}/\text{ns}$ is ~ 3 orders of magnitude larger than experimental values [24], reflecting the idealized ballistic regime and suggesting a mean free time on the order of 1.5 fs.

We define the strain-induced mobility as the response of the velocity to the applied force $\eta_\varepsilon(t) = \vec{v}_{drift}(t) \cdot \nabla_{\vec{r}}\varepsilon(t)$. This can be, generally, expressed as a simple power law $\vec{r}(t) \propto t^\alpha$, where the value of α determines the regime of the motion. $\alpha = 1$ corresponds to a, constant-motion, purely ballistic propagation, values of $\alpha < 1$ correspond to sub-ballistic drift, and values of $\alpha > 1$ correspond to super-ballistic drift. A special case of notice is $\alpha = 2$, which corresponds to propagation under a constant force. Figure 3 shows the power laws resulting from the time dependence of the mobility. To understand the effect of the various initial states and strain profiles on the mobility, the results are shown using box plots, and the different simulations were aggregated according to combinations of pairs of such conditions. Further details on this processing are provided in the SI. Although some simulations yield a slope of exactly 1 or 2, most fall between these values, with very few having a value lower than 1, and very few have values higher than 2. These results suggest that, predominantly, the exciton drift exhibits super-ballistic characteristics with a driving force that decreases with time. This behavior arises from the shape of the dispersion relations and their dependence on strain, which results in the addition of both accelerating and damping effective forces. Notably, although the shape of the strain profile and the initial position on the profile have a large effect on the drift regime, the initial momentum width has a negligible effect.

A particularly intriguing aspect of exciton transport in strained TMDs is the emergence of anomalous diffusion regimes, including reports of so-called negative diffusion, where exciton distributions appear to contract rather than broaden over time. While proper diffusion typically arises from interparticle interactions, ballistic broadening contributes to the overall

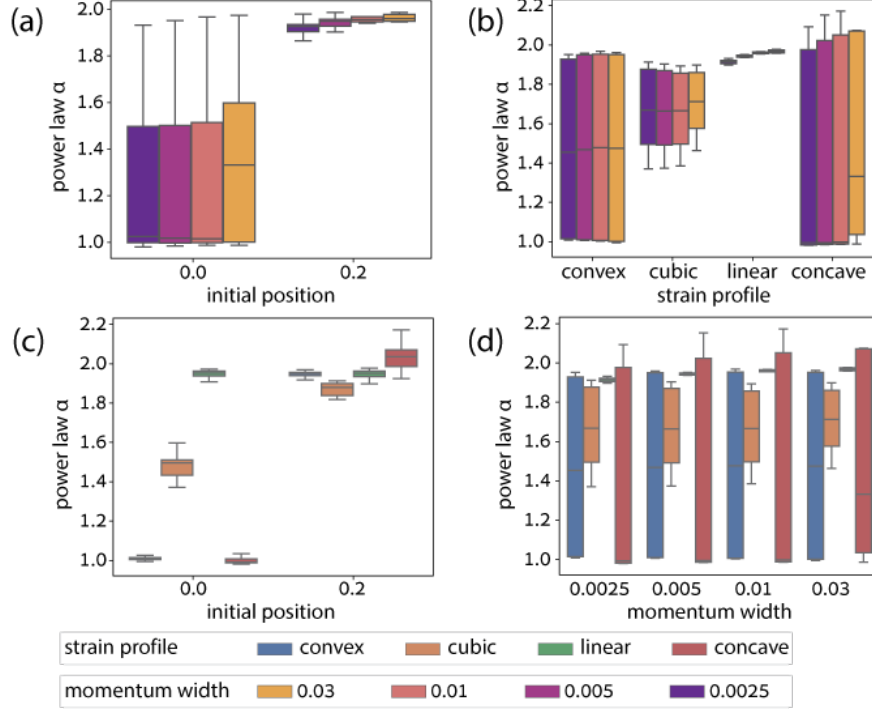


FIG. 3. Box plot of the strain-induced mobilities resulting under (a) various initial positions with solutions grouped by initial width of momentum distribution, (b) various strain profiles with solutions grouped by initial width of momentum distribution, (c) various initial positions with solutions groups by shape of strain profile, (d) various initial width of momentum distribution with solutions groups by shape of strain profile. A purely ballistic propagation should result in linear mobility. Most strain profiles yield sub-ballistic transport behavior ($\alpha < 1$), but concave parabolic profiles in particular lead to ballistic or even super-ballistic regimes ($\alpha \approx 1^2$). The researched strain profiles are either *linear*, parabolic *concave*, parabolic *convex*, or *cubic* with respect to a position coordinate, as per equation 2.

spatial expansion and can serve as a proxy for interpreting such anomalous behaviors. In anisotropic strain landscapes, exciton distributions often become distorted, prompting us to analyze the time evolution of distribution widths projected along orthogonal directions, where the profiles remain approximately Gaussian throughout propagation.

In the absence of strain, exciton broadening follows the expected ballistic trend—where the square of the spatial width scales linearly with the square of time—for all initial momentum-space widths. The slope of this relationship depends on the initial spread in momentum space, consistent with semiclassical expectations. Under nonzero strain, how-

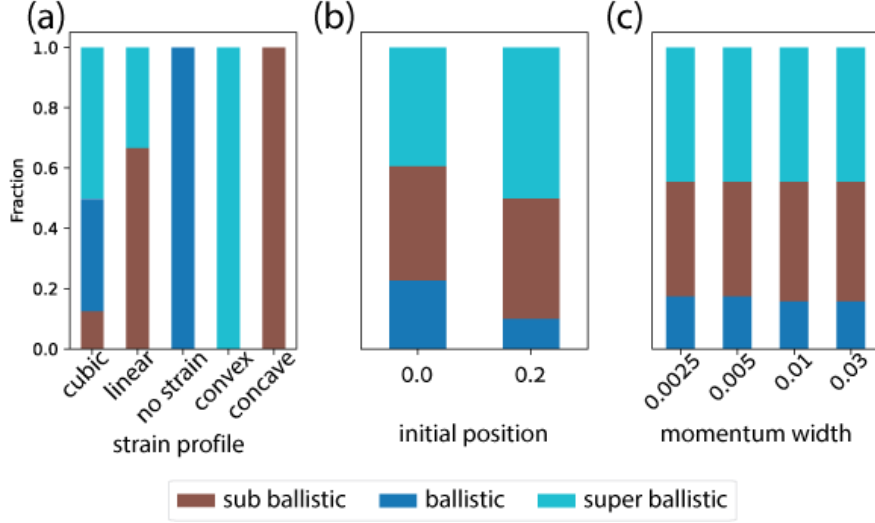


FIG. 4. Behavior of the time evolution of position-space width under (a) various strain profile shapes, (b) various initial positions, and (c) various initial momentum widths. Without strain, the time-evolution of the position-space width behaves as a ballistic expansion. Concave strain profiles always result in a sub-ballistic expansion, which is related to negative diffusion regimes. Convex strain profiles always result in super-ballistic expansion. Linear strain profiles can induce either sub- or super-ballistic expansions depending on initial conditions, while cubic profiles can exhibit all three expansion behaviors. Both the sub-ballistic and super-ballistic regimes correspond to anomalous diffusion regimes when interparticle interactions are considered.

ever, the broadening deviates from this ideal. To classify these deviations, we introduce a normalized width by comparing each strained system to its corresponding unstrained counterpart. A normalized width greater than one indicates super-ballistic broadening; values below one indicate sub-ballistic behavior.

Figure 4 presents the frequency of these regimes across different strain profiles, initial exciton positions, and momentum-space widths. The strain profile geometry emerges as the dominant factor shaping the broadening behavior, while the initial momentum width plays a negligible role. Parabolic strain profiles yield consistent behavior: convex profiles produce super-ballistic broadening, while concave profiles lead to sub-ballistic broadening. Linear strain profiles tend to exhibit super-ballistic broadening unless coupled with non-linearity in an orthogonal direction, which then suppresses the expansion. Cubic profiles display position-dependent behavior: excitons initialized in convex regions broaden super-

ballistically, while those in concave regions are sub-ballistic. At inflection points, broadening is approximately ballistic.

Strikingly, combinations of sub-ballistic broadening and suppressed drift in the same direction give rise to negative broadening. These results provide microscopic insight into the possible origin of anomalous and negative diffusion observed in experiments, and demonstrate how the geometry of the strain landscape can be harnessed to control exciton transport in 2D materials.

To conclude, we have developed a fully first-principles-based semiclassical framework for modeling the time evolution of macroscopic distributions of quasiparticle distributions on inhomogeneously strained monolayer semiconductors. Applied to strained WS_2 monolayers with idealized polynomial strain profiles, our model captures the qualitative impact of band curvature and energy gradients on exciton drift and diffusion, in the absence of scattering and relaxation mechanisms. The model qualitatively reproduces experimentally observed behaviors such as drift toward strain maxima, anisotropic broadening, and negative diffusion. It also provides a physical basis for estimating the ballistic mean free time in idealized regimes. These results offer fundamental insight into how strain modulates exciton transport in 2D semiconductors and establish a foundation for ab initio-informed design principles in straintronic devices, where strain landscapes are engineered to control quasiparticle motion. The model allows for straightforward incorporation of exciton interactions, enabling the method to evolve toward predictive modeling of realistic transport in complex strain landscapes.

Acknowledgments: We thank Moshe Haratz, Lev Melnikovski, and Galit Cohen for valuable discussions. Computational resources were provided by the ChemFarm local cluster at the Weizmann Institute of Science and the Max Planck Computing and Data Facility cluster. This research was supported by a European Research Council (ERC) Starting Grant (No. 101041159).

COMPUTATIONAL DETAILS

The starting point for constructing the position- and momentum-dependent exciton potential is a series of monolayer WS_2 systems, each subjected to uniform strain by modifying the unit cell dimensions and internal atomic coordinates accordingly. Tensile strain is ap-

plied by enlarging (positive change) the unit cell, while compressive strain is applied by shrinking (negative change) the unit cell. These changes can be applied to a single in-plane crystal axis, resulting in uniaxial strain; to both in-plane crystal axes, resulting in uniform strain; or to the out-of-plane axis, resulting in out-of-plane strain. In this work we focus on the study of uniform strains as an illustrative example. The atomic geometry of the unit cells remains unchanged after their modification, since this procedure can induce coupling between different strain modes, which we aim to avoid in this study.

For each strained configuration, we perform Density Functional Theory (DFT) calculations, followed by a calculation of the quasiparticle (QP) corrections within many-body perturbation theory at the G_0W_0 (GW) approximation. The exciton band structure is then obtained by solving the Bethe-Salpeter equation (BSE), yielding the momentum-resolved exciton energies required for our dynamics model. Full computational details are given in the SI.

DATA AVAILABILITY

The raw exciton band structure data generated and utilized in this study is available as part of the code base at the public github repository https://github.com/amirkl91/strain_dynamics with <https://doi.org/10.5281/zenodo.15855463>.

CODE AVAILABILITY

All code utilized to generate potential surfaces and solve dynamics model is available from the public github repository https://github.com/amirkl91/strain_dynamics with <https://doi.org/10.5281/zenodo.15855463>.

-
- [1] Mak, K. F., Lee, C., Hone, J., Shan, J. & Heinz, T. F. Atomically Thin MoS₂: A New Direct-Gap Semiconductor. *Phys. Rev. Lett.* **105**, 136805 (2010).
 - [2] Yun, W. S., Han, S. W., Hong, S. C., Kim, I. G. & Lee, J. D. Thickness and strain effects on electronic structures of transition metal dichalcogenides: 2H-M₂X₂ semiconductors (M = Mo, W; X = S, Se, Te). *Phys. Rev. B* **85**, 033305 (2012).

- [3] Refaely-Abramson, S., Qiu, D. Y., Louie, S. G. & Neaton, J. B. Defect-Induced Modification of Low-Lying Excitons and Valley Selectivity in Monolayer Transition Metal Dichalcogenides. *Phys. Rev. Lett.* **121**, 167402 (2018).
- [4] Amit, T., Hernangómez-Pérez, D., Cohen, G., Qiu, D. Y. & Refaely-Abramson, S. Tunable magneto-optical properties in $\{\mathrm{MoS}\}_2$ via defect-induced exciton transitions. *Phys. Rev. B* **106**, L161407 (2022).
- [5] Hernangómez-Pérez, D., Kleiner, A. & Refaely-Abramson, S. Reduced Absorption Due to Defect-Localized Interlayer Excitons in Transition-Metal Dichalcogenide–Graphene Heterostructures. *Nano Lett.* **23**, 5995–6001 (2023).
- [6] Geim, A. K. & Grigorieva, I. V. Van der Waals heterostructures. *Nature* **499**, 419–425 (2013).
- [7] Latini, S., Olsen, T. & Thygesen, K. S. Excitons in van der Waals heterostructures: The important role of dielectric screening. *Phys. Rev. B* **92**, 245123 (2015).
- [8] Zeng, Q. & Liu, Z. Novel Optoelectronic Devices: Transition-Metal-Dichalcogenide-Based 2D Heterostructures. *Adv. Electron. Mater.* **4**, 1700335 (2018).
- [9] Kleiner, A., Hernangómez-Pérez, D. & Refaely-Abramson, S. Designable exciton mixing through layer alignment in WS₂-graphene heterostructures. *npj 2D Mater Appl* **8**, 1–7 (2024).
- [10] Kundu, S., Naik, M. H., Krishnamurthy, H. R. & Jain, M. Moiré induced topology and flat bands in twisted bilayer $\{\mathrm{WSe}\}_2$: A first-principles study. *Phys. Rev. B* **105**, L081108 (2022).
- [11] Merkl, P. *et al.* Ultrafast transition between exciton phases in van der Waals heterostructures. *Nat. Mater.* **18**, 691–696 (2019).
- [12] Feng, J., Qian, X., Huang, C.-W. & Li, J. Strain-engineered artificial atom as a broad-spectrum solar energy funnel. *Nature Photon* **6**, 866–872 (2012).
- [13] Ghorbani-Asl, M., Borini, S., Kuc, A. & Heine, T. Strain-dependent modulation of conductivity in single-layer transition-metal dichalcogenides. *Phys. Rev. B* **87**, 235434 (2013).
- [14] Shi, H., Pan, H., Zhang, Y.-W. & Yakobson, B. I. Quasiparticle band structures and optical properties of strained monolayer MoS₂ and WS₂. *Phys. Rev. B* **87**, 155304 (2013).
- [15] Desai, S. B. *et al.* Strain-Induced Indirect to Direct Bandgap Transition in Multilayer WSe₂. *Nano Lett.* **14**, 4592–4597 (2014).
- [16] Deilmann, T. & Thygesen, K. S. Finite-momentum exciton landscape in mono- and bilayer transition metal dichalcogenides. *2D Mater.* **6**, 035003 (2019).

- [17] Guzman, D. M. & Strachan, A. Role of strain on electronic and mechanical response of semiconducting transition-metal dichalcogenide monolayers: An ab-initio study. *J. Appl. Phys.* **115**, 243701 (2014).
- [18] Zollner, K., Junior, P. E. F. & Fabian, J. Strain-tunable orbital, spin-orbit, and optical properties of monolayer transition-metal dichalcogenides. *Phys. Rev. B* **100**, 195126 (2019).
- [19] Sharma, M., Kumar, A., Ahluwalia, P. K. & Pandey, R. Strain and electric field induced electronic properties of two-dimensional hybrid bilayers of transition-metal dichalcogenides. *J. Appl. Phys.* **116**, 063711 (2014).
- [20] Wang, W. & Ma, X. Strain-Induced Trapping of Indirect Excitons in MoSe₂/WSe₂ Heterostructures. *ACS Photonics* **7**, 2460–2467 (2020).
- [21] Wang, Y. *et al.* Strain-induced direct–indirect bandgap transition and phonon modulation in monolayer WS₂. *Nano Res.* **8**, 2562–2572 (2015).
- [22] Defo, R. K. *et al.* Strain dependence of band gaps and exciton energies in pure and mixed transition-metal dichalcogenides. *Phys. Rev. B* **94**, 155310 (2016).
- [23] Khatibi, Z. *et al.* Impact of strain on the excitonic linewidth in transition metal dichalcogenides. *2D Mater.* **6**, 015015 (2018).
- [24] Cordovilla Leon, D. F., Li, Z., Jang, S. W., Cheng, C.-H. & Deotare, P. B. Exciton transport in strained monolayer WSe₂. *Applied Physics Letters* **113**, 252101 (2018).
- [25] Moon, H. *et al.* Dynamic Exciton Funneling by Local Strain Control in a Monolayer Semiconductor. *Nano Lett.* **20**, 6791–6797 (2020).
- [26] Datta, K. *et al.* Spatiotemporally controlled room-temperature exciton transport under dynamic strain. *Nat. Photon.* **16**, 242–247 (2022).
- [27] Kim, J. M. *et al.* Strained two-dimensional tungsten diselenide for mechanically tunable exciton transport. *Nat Commun* **15**, 10847 (2024).
- [28] Castellanos-Gomez, A. *et al.* Local Strain Engineering in Atomically Thin MoS₂. *Nano Lett.* **13**, 5361–5366 (2013).
- [29] Dirnberger, F. *et al.* Quasi-1D exciton channels in strain-engineered 2D materials. *Sci. Adv.* **7**, eabj3066 (2021).
- [30] Li, Z. *et al.* Enhanced Exciton Drift Transport through Suppressed Diffusion in One-Dimensional Guides. *ACS Nano* **17**, 22410–22417 (2023).

- [31] Harats, M. G., Kirchhof, J. N., Qiao, M., Greben, K. & Bolotin, K. I. Dynamics and efficient conversion of excitons to trions in non-uniformly strained monolayer WS₂. *Nat. Photonics* **14**, 324–329 (2020).
- [32] Rosati, R. *et al.* Strain-dependent exciton diffusion in transition metal dichalcogenides. *2D Mater.* **8**, 015030 (2020).
- [33] Uddin, S. Z. *et al.* Neutral Exciton Diffusion in Monolayer MoS₂. *ACS Nano* **14**, 13433–13440 (2020).
- [34] Wagner, K. *et al.* Nonclassical Exciton Diffusion in Monolayer WSe_2 . *Phys. Rev. Lett.* **127**, 076801 (2021).
- [35] Rosati, R., Perea-Causín, R., Brem, S. & Malic, E. Negative effective excitonic diffusion in monolayer transition metal dichalcogenides. *Nanoscale* **12**, 356–363 (2019).
- [36] Rosati, R. *et al.* Dark exciton anti-funneling in atomically thin semiconductors. *Nat Commun* **12**, 7221 (2021).
- [37] An, Z. *et al.* Strain control of exciton and trion spin-valley dynamics in monolayer transition metal dichalcogenides. *Phys. Rev. B* **108**, L041404 (2023).
- [38] Chand, S. B. *et al.* Visualization of Dark Excitons in Semiconductor Monolayers for High-Sensitivity Strain Sensing. *Nano Lett.* **22**, 3087–3094 (2022).
- [39] Hernández López, P. *et al.* Strain control of hybridization between dark and localized excitons in a 2D semiconductor. *Nat Commun* **13**, 7691 (2022).
- [40] Lee, H. *et al.* Drift-dominant exciton funneling and trion conversion in 2D semiconductors on the nanogap. *Sci. Adv.* **8**, eabm5236 (2022).
- [41] Qiu, D. Y., Cohen, G., Novichkova, D. & Refaely-Abramson, S. Signatures of Dimensionality and Symmetry in Exciton Band Structure: Consequences for Exciton Dynamics and Transport. *Nano Lett.* **21**, 7644–7650 (2021).
- [42] Koo, Y. *et al.* Tip-Induced Nano-Engineering of Strain, Bandgap, and Exciton Funneling in 2D Semiconductors. *Adv. Mater.* **33**, 2008234 (2021).
- [43] Mennel, L., Paur, M. & Mueller, T. Second harmonic generation in strained transition metal dichalcogenide monolayers: MoS₂, MoSe₂, WS₂, and WSe₂. *APL Photonics* **4**, 034404 (2018).
- [44] Kovalchuk, S., Kirchhof, Jan. N., Bolotin, K. I. & Harats, M. G. Non-Uniform Strain Engineering of 2D Materials. *Isr. J. Chem.* **62**, e202100115 (2022).
- [45] Bensmann, J. *et al.* Nanoimprint strain-engineering of 2D semiconductors (2022). 2212.11873.

- [46] Dhakal, K. P. *et al.* Local Strain Induced Band Gap Modulation and Photoluminescence Enhancement of Multilayer Transition Metal Dichalcogenides. *Chem. Mater.* **29**, 5124–5133 (2017).